FY19 National Laser Users' Facility Program

M. S. Wei

Laboratory for Laser Energetics, University of Rochester

During the second and third quarters of FY19, the National Nuclear Security Administration (NNSA) and the Office of Science jointly completed a funding opportunity announcement (FOA), review, and selection process for National Laser Users' Facility (NLUF) experiments to be conducted at the Omega Laser Facility during FY20 and FY21. Seventeen proposals were successfully submitted in response to this FOA. After peer review by an independent proposal review committee for scientific and technical merit and the feasibility review by the Omega Laser Facility team, NNSA selected 11 proposals for funding and Omega shot allocation with a total of 22.5 and 23.5 shot days for experiments in FY20 and FY21, respectively. It was noted that a large number of NLUF grant proposals failed during the initial administrative review due to unexpected submission errors and were deemed nonresponsive. Following NNSA's guidance, LLE made a one-time additional open-call late in FY19 to receive Omega Laser Facility time proposals for Academic and Industrial Basic Science (AIBS) experiments to fulfill the remaining NLUF shot allocation in FY20–FY21. Based on the merit review committee's recommendation, ten new projects were selected for Omega beam-time awards with a total of 11 and 10 shot days for AIBS experiments in FY20 and FY21, respectively. Table I shows the list of NLUF grant projects and AIBS beam-time awards approved for Omega shot allocations in FY20–FY21.

During the first and second quarters of FY19, eight NLUF projects that had been approved during the previous NLUF cycle (calendar year 2017–2018) completed 127 target shots. The NLUF experiments conducted at the facility during FY19 are summarized in this section.

A critical part of the NLUF program is the education and training of graduate students in plasma and HED physics. In addition, graduate students can also access the Omega Facility for shots through their collaborations with national laboratories and LLE. There were more than 60 graduate students from 18 universities involved in the external user-led research programs supported by NLUF/LBS and/or with experiments conducted at the Omega Laser Facility (see Table II), among which ten students successfully defended their Ph.D. theses during FY19 (see the highlighted names in Table II).

Structure of $MgSiO_3$ Under Ramp Compression to 368 GPa
Principal Investigator: T. S. Duffy (Princeton University)
Co-investigators: D. Kim and S. Han (Princeton); R. F. Smith and F. Coppari (LLNL), and J. K. Wicks (Johns Hopkins University)

In Earth's lower mantle, enstatite [$(Mg,Fe)SiO_3$] transforms into the perovskite-structured mineral known as bridgmanite. This phase is considered to be the most abundant mineral in the entire earth, making up as much as 80% of the volume of the vast lower mantle. Near the base of the mantle, bridgmanite undergoes a further phase transition to the post-perovskite (ppv, $CaIrO_3$-type) structure. The ppv phase is expected to play a major role in the interiors of large terrestrial exoplanets due to the higher internal pressures of these bodies. It is therefore necessary to understand the behavior of enstatite at extreme conditions to develop models for the mineralogy, structure, and dynamics of such exoplanets.

We carried out experiments on OMEGA on several different enstatite starting materials, including a low-Fe enstatite $\left[\mathrm{Mg}/(\mathrm{Mg}+\mathrm{Fe}) \sim 0.99\right]$ from Sri Lanka, a high-Fe enstatite $\left[\mathrm{Mg}/(\mathrm{Mg}+\mathrm{Fe}) \sim 0.61\right]$ from India, and a synthetic $MgSiO_3$ glass

(MDI, Inc.). All samples were ground to a few microns in size, pressed into a foil using a diamond-anvil cell, and assembled into target packages. Experiments were performed on both OMEGA and OMEGA EP using ramp compression and x-ray diffraction with the powder x-ray diffraction image-plate (PXRDIP) diagnostic. These experiments are especially challenging due to the relatively weak scattering and low symmetry of high-pressure silicate phases.

Table I: Eleven NLUF grant projects (in blue) and ten AIBS beam-time awards (in gray) approved for the FY20–FY21 Omega Laser Facility shot allocations.

Principal Investigator	Institution	Title
F. N. Beg	University of California, San Diego	Charged-Particle Transport and Energy Deposition in Warm Dense Matter With and Without an External Magnetic Field
C. M. Krauland	General Atomics	Characterization of the Nonlinear Laser–Plasma Interaction in Electron-Assisted Shock Ignition
K. Krushelnick	University of Michigan	The Dynamics of Strong Magnetic Fields Generated by Relativistic Laser–Plasma Interactions Using OMEGA EP
E. Liang	Rice University	Collision of Two Magnetized Jets Created by Hollow Ring Lasers
R. Mancini	University of Nevada, Reno	A Laboratory Photoionized Plasma Experiment on OMEGA EP
C. McGuffey	University of California, San Diego	Driving Compressed Magnetic Fields to Exceed 10 kT in Cylindrical Implosions on OMEGA
R. Petrasso	Massachusetts Institute of Technology	High-Energy-Density Physics, Laboratory Astrophysics, and Student Training on OMEGA
P. Tzeferacos	University of Chicago	Fundamental Astrophysical Processes in Radiative Supersonic MHD Turbulence
M. Vaddivia	Johns Hopkins University	Demonstration of Monochromatic Talbot–Lau X-Ray Deflectometry (TXD) Electron Density Diagnostic in Laser–Target Interactions
J. Wicks	Johns Hopkins University	High Pressure and Temperature Polymorphism of a Key Super-Earth Mantle Material: MgO
L. Willingale	University of Michigan	Direct Laser Acceleration of Electrons for Bright, Directional Radiation Sources
M. Cappelli	Stanford University	Hydrodynamic versus Kinetic Atomic Mix in Deflagrating Converging Plasmas
T. Duffy	Princeton University	Phase Transitions in Planetary Materials at Ultrahigh Pressures
W. Fox	Princeton University	Magnetic Reconnection in High-Energy-Density Plasmas
R. Jeanloz	University of California, Berkeley	Multi-Compression and Chemical Physics of Planetary Interiors
H. Ji	Princeton University	Study of Particle Acceleration from Magnetically Driven Collisionless Reconnection at Low Plasma Beta Using Laser-Powered Capacitor Coils
C. Kuranz	University of Michigan	Experimental Astrophysics on the OMEGA Laser
M. Manuel	General Atomics	B-Field Effects on Laser–Plasma Instabilities
D. Schaeffer	Princeton University	Particle Heating by Collisionless Shocks in Magnetized High-Energy-Density Plasmas
B. Srinivasan	Virginia Tech	Investigation of Feasibility of the 11B(P,3α) Reaction in ICF Settings
W. Theobald	University of Rochester	Quantifying Turbulent Rayleigh–Taylor Mixing with X-Ray Phase Contrast Imaging

Table II: Graduate students from other universities who have conducted research utilizing the Omega Laser Facility through NLUF and LBS or via collaborations with national laboratories and LLE in FY19. Ten students successfully defended their Ph.D. thesis during FY19 (see shaded cells).

Name	University	Academic Advisor	Notes
Patrick Adrian	MIT	Petrasso	
Timothy Mark Johnson	MIT	Petrasso	
Neel Kabadi	MIT	Petrasso	
Justin Kunimune	MIT	Petrasso	
Brandon Lahmann	MIT	Petrasso	
Jacob Pearcy	MIT	Petrasso	
Raspberry Simpson	MIT	Petrasso	
Benjamin Reichelt	MIT	Petrasso	
Hong Sio	MIT	Petrasso	Graduated October 2018; postdoc at LLNL
Graeme Sutcliffe	MIT	Petrasso	
Abraham Chien	Princeton	Ji	
Cole Holcomb	Princeton	Spitkovsky	Graduated December 2018; data scientist at The Estée Lauder Companies
Jack Matteucci	Princeton	Bhattacharjee/Fox	Graduated January 2020
Donghoon Kim	Princeton	Duffy	
Sirus Han	Princeton	Duffy	
Ian Ocampo	Princeton	Duffy	New
Connor Krill	JHU	Wicks	New; through LLNL-led LBS
Juliette Lamoureux	JHU/NASA Goddard	Wicks	New
Tylor Perez	JHU	Wicks	New
Zixuan Ye	JHU	Wicks	New
Melissa Sims	Stonybrook	Wicks	Defended in March 2019; postdoc at JHU
Dylan Cliché	University of Nevada, Reno	Mancini	LLE collaboration
Enac Gallardo	University of Nevada, Reno	Mancini	LLE collaboration
Daniel Mayes	University of Nevada, Reno	Mancini	
Kyle Swanson	University of Nevada, Reno	Mancini	
Patrick Belancourt	University of Michigan	Drake	Through collaboration with LLE including LBS shots
Shane Coffing	University of Michigan	Drake/Kuranz	
Laura Elgin	University of Michigan	Drake/Kuranz	Through collaboration with national labs; graduated September 2019; postdoc at SNL
Raul Melean	University of Michigan	Kuranz/McBride	Collaboration with JHU's NLUF (P. Valdivia)
Heath Lefevre	University of Michigan	Kuranz/Drake	
Joseph Levesque	University of Michigan	Drake/Kuranz	

Table II: Graduate students from other universities who have conducted research utilizing the Omega Laser Facility through NLUF, LBS, or via collaborations with national labs and LLE in FY19. Ten students successfully defended their Ph.D. thesis during FY19 (see shaded cells) (continued).

Name	University	Academic Advisor	Notes
Alex Rusmas	University of Michigan	Kuranz/Drake	Through collaboration with. LANL; defended in April 2019, now a postdoc at LANL
Robert Vandervort	University of Michigan	Drake	
Paul Campbell	University of Michigan	Krushelnick/Willingale	Defended October 2019; now a FES Postdoc Fellow at the University of Michigan
Amina Hussein	University of Michigan	Krushelnick/Willingale	Defended in June 2019; now UC President Postdoc Fellow
Peter Kordell	University of Michigan	Krushelnick	Defended in May 2019; now at Northrop Grumman
Brandon Russell	University of Michigan	Krushelnick/Willingale	
Hongmei Tang	University of Michigan	Krushelnick/Willingale	New
Krish Bhutwala	University of California, San Diego	Beg	
Rui Hua	University of California, San Diego	Beg	Through LLNL-led LBS (PI Ping); defended in September 2019; imaging scientist at Cannon Medical Research USA
Shu Zhang	University of California, San Diego	Beg	Through GA-led NLUF
Kaitlyn Amodeo	University of California, Davis	Stewart	Through LLNL-led LBS (PI Millot)
Erik Davies	University of California, Davis	Stewart	Through LLNL-led LBS (PI Millot)
Paul King	University of Texas, Austin	Hegelich	Through LLNL-led LBS (PI Albert)
Dara Hok	Stanford	Gleason-Holbrook	Through LLNL-led LBS (PI Krygier)
Yongchao Lu	Rice University	Liang	Rice-led NLUF and also through LANL collaboration
Kevin Meaney	University of New Mexico	Gilmore	Through LANL collaboration
Brett Scheiner	University of Iowa	Baalrud	Through LANL collaboration
Oliver Vaxirani	Virginia Tech	Srinivasan	Through LANL collaboration
Archie Bott	Oxford	Gregori	Through University of Chicago-led NLUF (PI Lamb); graduated 2019; postdoc at Princeton University
Oliver Karnbach	Oxford	Gregori/Wark	Through LLNL-led LBS (PI Chen)
Hannah Poole	Oxford	Gregori	Collaboration with LLE
Jacob Topp-Mytflestone	Oxford	Gregori	Collaboration with LLE
Gabriel Perez-Callejo	Oxford	Rose	Through LLNL-led LBS and HED (PI Marley)

Table II: Graduate students from other universities who have conducted research utilizing the Omega Laser Facility through NLUF, LBS, or via collaborations with national labs and LLE in FY19. Ten students successfully defended their Ph.D. thesis during FY19 (see shaded cells) (continued).

Name	University	Academic Advisor	Notes
Jocelain Trela	University of Bordeaux	Batani	Through LLE-led LBS (PI Theobald); graduated June 2019; scientist at CEA
Matthew Khan	University of York	Woolsey	Through LLE-led LBS (PI Theobald)
Gabriel Rion	Ecole Polytechnique, Palaiseau		Through LLE-led LBS (PI Theobald)
Victorien Bouffetier	University of Bordeaux		Through LLE-led LBS (PI Theobald) and JHU-led NLUF
Olena Turianska	University of Bordeaux		Through LLE-led LBS (PI: Theobald)
Thibault Goudai	University of Bordeaux		Through LLNL-led LBS (PI: Khan)

JHU: Johns Hopkins University
MIT: Massachusetts Institute of Technology

Nine successful experiments have been conducted in total (five Fe-poor, two Fe-rich, and two $MgSiO_3$ glass). For the crystalline samples, the drive energies ranged from 207 to 597 J and the resulting pressures were 118 to 277 GPa. The experiments used Cu or Fe backlighters paired with pinholes made from W or Ta. For the glass samples, the drive energies ranged from 607 to 912 J and the resulting pressures were 274 to 368 GPa. In the experiments on the crystalline samples, one to three sample diffraction lines were observed in seven shots. The diffraction lines from all shots produced a consistent *d* spacing trend as a function of pressure, and all samples yielded diffraction lines with similar *d* spacings, suggesting transformation to the same phase. Interestingly, the positions of the observed diffraction lines are not consistent with the major peaks of the post-perovskite phase, which is expected to be stable at these pressures. The peaks are also not consistent with bridgmanite or akimotoite, two forms of (Mg,Fe) SiO_3 stable under lower pressure conditions. We commenced a search among metastable $MgSiO_3$ phases that have been reported in diamond-anvil cell experiments and obtained a tentative match with a phase known as β-postopx (post-orthopyroxene). Our group had previously observed this phase in single-crystal, 300-K diamond anvil cell experiments above 50 GPa. The structure consists of alternating Mg-O and Si-O layers. The Mg-O layers are pyroxene-like, whereas the Si-O layers transform toward akimotoite-like sheets with 4 + 1 and sixfold coordination of silicon with oxygen.

Our results (Fig. 1) indicate that ramp compression of a silicate at 1 to 2 Mbar may produce a metastable phase. Furthermore, it indicates that the same high-pressure phases may be generated in low-temperature static experiments and rapid dynamic experiments, further demonstrating the complementarity of the two techniques. Our results also show that we can potentially place constraints on high-pressure phases in weakly diffracting, low-symmetry silicate systems under extreme pressures. Future experiments will be aimed at better constraining the crystal structure by enhancing the diffraction signal. X-ray diffraction under shock compression will also be performed to compare structures obtained under different loading conditions.

This material is based upon work supported by the Department of Energy National Nuclear Security Administration through the National Laser Users Facility Program under Award Number DE-NA0003611.

Properties of Magnetohydrodynamic Turbulence in Laser-Produced Plasmas

Principal Investigator: D. Lamb University of Chicago
Co-investigators: G. Gregori and P. Tzeferacos (University of Chicago and Oxford University); C. Palmer, A. Bott, L. Chen, and J. Meinecke (Oxford); D. H. Froula and J. Katz (LLE); H.-S. Park (LLNL); and R. D. Petrasso, C. K. Li, and A. Birkel (MIT)

Astronomical observations that are based on Faraday rotation and polarization measurements, the Zeeman effect, magneto-bremsstrahlung, and *in-situ* measurements of proximal astrophysical objects reveal how space is permeated by magnetic fields[1] that play crucial roles in myriad astrophysical phenomena. Despite the broad consensus among astronomers that magnetic-field

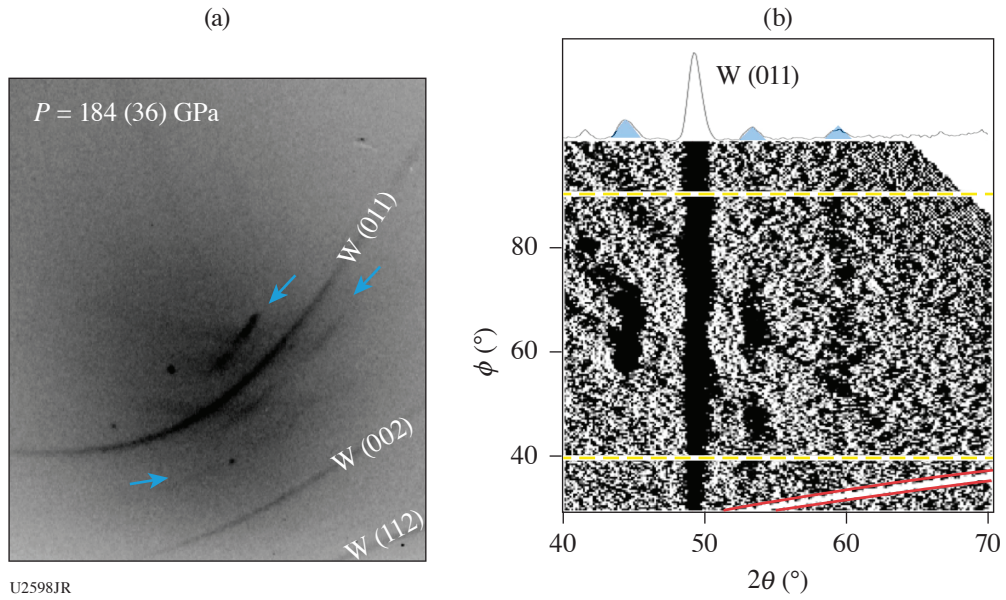

Figure 1
Diffraction data for $MgSiO_3$ at 183(36) GPa. (a) One of the image plates for OMEGA EP shot 27426. Lines from the enstatite sample are indicated by blue arrows. (b) Image-plate data transformed to ϕ–2θ coordinates, where ϕ is the azimuthal angle around the incident x-ray beam and 2θ is the diffraction angle. A lineout from the region between the yellow horizontal dashed lines is shown at the top. Peaks from the high-pressure phase of $MgSiO_3$ are shaded in blue.

amplification via turbulent dynamo is behind observed cosmic magnetism, theoretical considerations and numerical modeling have unavoidably resorted to simplifying assumptions that do not necessarily reflect the properties of astrophysical turbulence. Turbulent dynamo theoretical and numerical studies have largely focused on incompressible turbulence, and simulations are typically restricted to magnetic Prandtl numbers Pm ~ 1 due to resolution constraints,[2] rarely considering systems of equations that go beyond resistive magnetohydrodynamics (MHD). Only in the last few years have theoretical and numerical efforts begun to tackle highly compressible magnetized turbulence[3,4]—an important step forward, given that most astrophysical systems in the interstellar and intergalactic mediums exhibit signs of high compressibility [i.e., large sonic Mach (M) numbers]. Supersonic turbulence plays a critical role in determining the star formation rate,[5] the star formation efficiency,[6] and the stellar mass distribution.[7]

Supersonic magnetized turbulence and turbulent dynamo were the astrophysical processes we targeted on the third shot day of the TDYNO NLUF Experimental Campaign, "Properties of Magnetohydrodynamic Turbulence in Laser-Produced Plasmas." The shot day was carried out on 12 December 2018 and included the 30,000th shot of OMEGA, an important facility milestone. We prototyped and deployed a platform [Fig. 2(a)] similar to the one we fielded on OMEGA for our previous successful TDYNO Campaigns (FY15–FY18), during which we (1) demonstrated nonlinear amplification by turbulent dynamo for the first time in a laboratory environment;[8,9] (2) quantified the diffusion of energetic charged particles through magnetized turbulence;[10] and (3) characterized the growth rates in the kinematic and nonlinear phases of the turbulent dynamo mechanism.[11] Guided by simulation campaigns using the *FLASH* code[12–15] [Fig. 2(b)] on one of the nation's leadership supercomputers, we modified the original TDYNO platform to achieve supersonic turbulence. The configuration consists of two diametrically opposed chlorinated CH foil targets and a pair of grids supported by cylindrical shields. The foil targets are backlit with temporally stacked beams, delivering 5 kJ of energy on each side in a 5-ns ramp-up. The beams drive a pair of counter-propagating, high-Rm plasma flows that carry the seed magnetic fields generated by a Biermann battery. The flows propagate through a pair of grids that destabilize the flow and define the driving scale of the turbulence. The flows then meet at the center of the chamber to form a hot, turbulent interaction region where the magnetic fields are amplified to saturation values [Fig. 2(c)]. The chlorine dopant increases the radiative cooling efficiency of the turbulent plasma. This results in a decrease in the temperature and the sound speed of the plasma, making it supersonic [Fig. 2(d)]. However, our design enabled us to retain high-enough temperatures in the turbulent plasma to achieve supercritical Rm values for dynamo to operate [Fig. 2(e)].

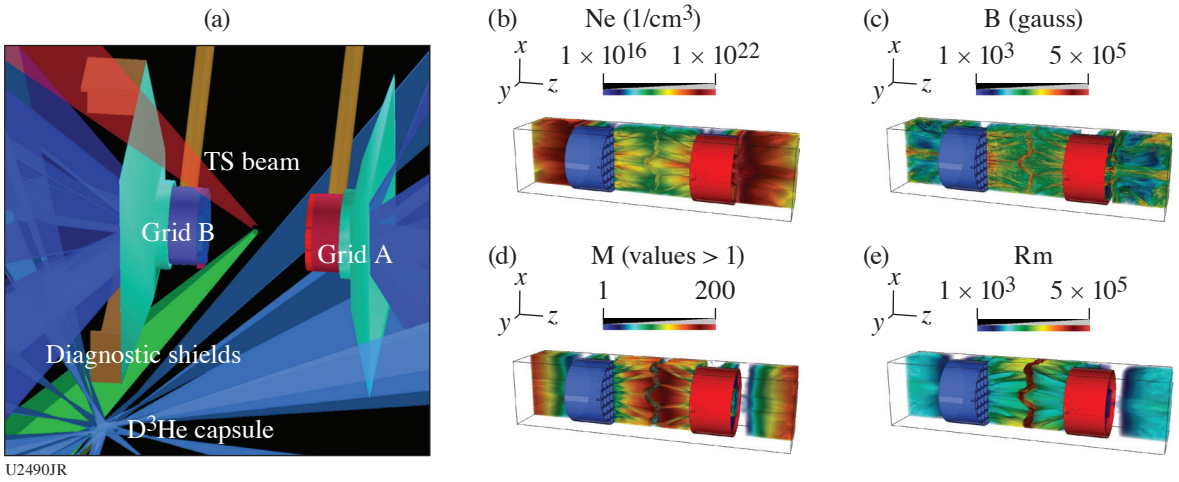

Figure 2
Supersonic turbulent dynamo on OMEGA. (a) VisRad schematic of the supersonic TDYNO platform for OMEGA. (b) *FLASH* simulation of the CHCl platform we will field on OMEGA (electron number density rendering). (c) Magnetic-field strength in the *FLASH* simulation, indicating amplification to hundreds of kG. (d) Mach number of the plasma flows and the turbulent region, showing only values above unity. The turbulent plasma is robustly supersonic. (e) The Rm values in the *FLASH* simulations are above RmC, in the many hundreds.

The primary goals of this shot day were to determine the energy cascade of the supersonic MHD turbulence by measuring the spectrum of both the magnetic field and plasma fluctuations and to characterize and map out the time history and saturation of turbulent dynamo in the supersonic regime. The shots yielded a wealth of experimental data, and preliminary analysis indicates that we were, in fact, able to generate compressible magnetized turbulence, characterize the plasma state, and measure the magnetic-field amplification using the suite of diagnostics we fielded previously. More specifically, we used x-ray imaging [Fig. 3(a)] to visualize the formation and evolution of the magnetized turbulence and to reconstruct the density power spectrum from the x-ray intensity fluctuations [Fig. 3(b)]. Moreover, the 4ω Thomson-scattering diagnostic yielded detailed information on the plasma state (ion and electron temperatures, bulk flow velocity, turbulent velocity, and electron density) at different times. During this first attempt at a 4ω probe, the diagnostic performed remarkably well. Finally, we employed proton radiography [Fig. 4(a)] on all shots and reconstructed the path-integrated magnetic fields[16,17] [Fig. 4(b)], thereby measuring the magnetic-field amplification.

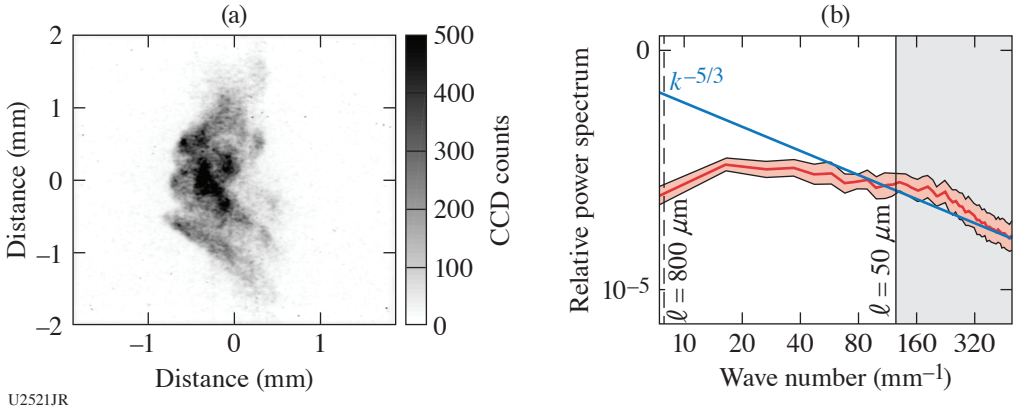

Figure 3
(a) X-ray image of supersonic radiative turbulence on OMEGA. (b) The shallow power spectrum from the x-ray fluctuations of (a) shows a departure from Kolmogorov and more power at small scales, consistent with supersonic turbulence.

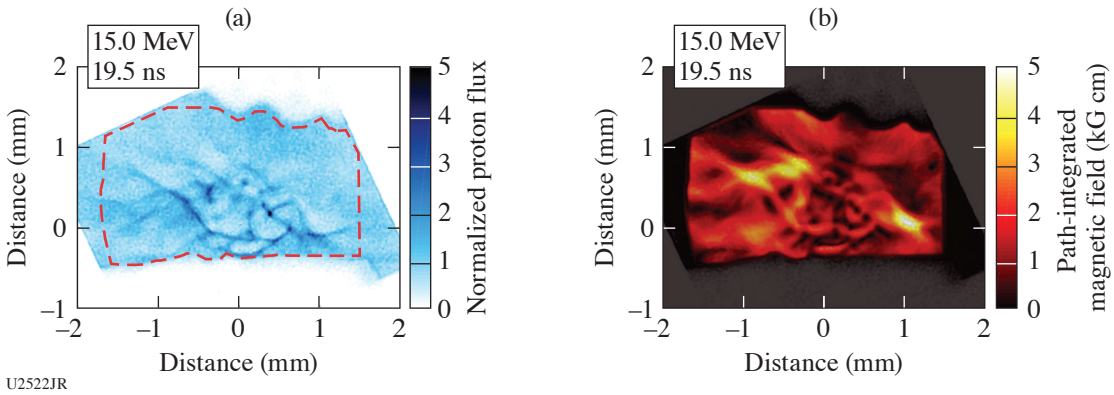

Figure 4
(a) Proton radiography of the turbulent interaction region at the same time as Fig. 3(a). (b) Path-integrated magnetic field from the proton radiograph in (a).

Despite the complexity of the experimental platform, the alignment procedures we developed, with the help of personnel from LLE and General Atomics, enabled us to perform 14 shots during our third shot day. The experimental data are currently being analyzed and promise to further our understanding of magnetized astrophysical turbulence in the supersonic regime.

The research leading to these results has received funding from the European Research Council under the European Community's Seventh Framework Programme (FP7/2007-2013)/ERC grant agreements no. 256973 and 247039, the U.S. Department of Energy under Contract No. B591485 to Lawrence Livermore National Laboratory, Field Work Proposal No. 57789 to Argonne National Laboratory, Subcontract No. 536203 with Los Alamos National Laboratory, Subcontract B632670 with Lawrence Livermore National Laboratory, and grants no. DE-NA0002724, DE-NA0003605, and DE-SC0016566 to the University of Chicago. We acknowledge support from the National Science Foundation under grants PHY-1619573 and PHY-1903430. Awards of computer time were provided by the U.S. Department of Energy ASCR Leadership Computing Challenge (ALCC) program. This research used resources of the Argonne Leadership Computing Facility at Argonne National Laboratory, which is supported by the Office of Science of the U.S. Department of Energy under contract DE-AC02-06CH11357. Support from AWE plc., the Engineering and Physical Sciences Research Council (grant numbers EP/M022331/1, EP/N014472/1 and EP/P010059/1) and the Science and Technology Facilities Council of the United Kingdom is also acknowledged, as well as funding from grants 2016R1A5A1013277 and 2017R1A2A1A05071429 of the National Research Foundation of Korea. This material is based upon work supported by the Department of Energy National Nuclear Security Administration under Award Number DE-NA0003856, the University of Rochester, and the New York State Energy Research and Development Authority.

An Experiment to Observe Photoionization Fronts in the Laboratory

Principal Investigator: H. J. LeFevre (University of Michigan)
Co-investigators: W. J. Gray, J. S. Davis, R. Gillespie, S. R. Klein, C. C. Kuranz, and R. P. Drake (University of Michigan); and P. A. Keiter (LANL)

When there is a sustained ionizing radiation source incident on a medium, such as the end of the cosmic dark ages and present-day star-forming regions, heat fronts propagate out from the source until the heating and cooling rate reach a steady state.[18] In the examples from cosmology and astrophysics listed above, photoionization (PI) is the process driving the heating, and the heat front formed is called a PI front. PI-front physics is also relevant to the capsule implosions in indirect-drive inertial confinement fusion experiments. Since there has been no observation of this type of front in astrophysics or the laboratory, an experiment to understand their properties is of interest.

Work by Drake and Gray[19,20] shows that it is possible to generate the appropriate conditions for a PI front using a laser-irradiated Au foil[21] on the OMEGA laser. They parameterize the experiment to the atomic physics of the problems with two dimensionless parameters:

$$\alpha = \frac{n_{i+1}}{n_i}\,\frac{n_e R_{i+1,i}}{\Gamma_{i,i+1}}, \tag{1}$$

$$\beta = 1 + \frac{n_{\mathrm{i}}}{n_{\mathrm{i}+1}} \frac{\langle \sigma v \rangle_{\mathrm{i,i}+1}}{R_{\mathrm{i}+1,\mathrm{i}}}, \tag{2}$$

where n_{i} is the population density of the ith ionization state, n_{e} is the electron density, $R_{\mathrm{i+1,i}}$ is the total recombination rate, $\Gamma_{\mathrm{i,i+1}}$ is the photoionization rate, and $\langle \sigma v \rangle_{\mathrm{i,i+1}}$ is the electron collisional ionization rate. In order to produce a PI front, Eq. (1) must be much less than 1 and Eq. (2) should be ~1. An ~80-eV quasi-blackbody source possible on OMEGA[21] incident on an 8.5-atm N gas cell should be sufficient to drive a front that has dimensionless parameters in the correct regime.[19,20]

The gas cell used in these experiments had a 3-mm inner diameter and a 7-mm length with a 750-nm-thick plastic window supported by a 100-μm-thick stainless-steel grid and a 500-nm-thick Au foil with a 3-mm diameter that was 300 μm from the gas cell window. Ten beams using SG5 phase plates drive the Au foil with an intensity of 10^{14} W/cm^2 by using pairs of beams with 1-ns pulse shapes to create 5 ns of total drive duration.

The primary measurement in this experiment is absorption spectroscopy of a 1% Ar dopant in the N gas cell. Irradiating a glow-discharge polymer capsule with an 850-μm outer diameter and a 9-μm wall thickness using 20 beams each with a 1-ns square pulse shape implodes the capsule, which produces a 220-ps-duration, continuum x-ray source in the spectral range of the Ar K shell from 2.9 to 3.3 keV. The capsule location was 10 mm from the axis of the gas cell with a 100-μm W aperture offset by 5 mm to restrict the source-size broadening of the spectrum. This measurement will provide the temperature, density, and ionization states of the Ar dopant, which one would then correlate to the plasma parameters in the N. To measure the spectrum through the gas cell, an x-ray spectrometer (XRS) was fielded in a ten-inch manipulator (TIM-3) with a PET crystal in position 2 with a 4° tilt to a central angle of 19.56°. Another XRS in TIM-1 with the same crystal configuration pointed at an unobstructed surface of the crystal recorded the unattenuated spectrum on each shot. A framing camera in TIM-2 recorded the capsule source size during the x-ray flash, a soft x-ray framing camera in TIM-6 observed the capsule emission size from an about orthogonal view, and a framing camera in TIM-5 observed the front surface emission of the Au foil. Additionally, Dante ran on these shots to observe the time-resolved capsule flux and characterize the Au foil emission on a dedicated shot.

Of the nine total shots during the campaign, three types of null shots evaluated the noise sources present during the measurement: only capsule, only capsule with gas cell present, and only driven gas cell. The remaining six shots included a repeat capsule-only null shot and five integrated physics shots. This resulted in a thorough characterization of the capsule backlighter used as an absorption source. However, there were emission lines in the capsule data, shown in Fig. 5(a), caused by contaminants in the capsule that affected the data analysis on shot day. Additionally, the gas cell acts to collimate the capsule emission [shown in Figs. 5(b) and 5(c)], which limits the spectral range of the absorption measurement, and the anticipated Ar absorption lines lie outside this narrow range. The crystal tilt was meant to adjust for this collimation, but this configuration was not well constrained. As a result, the shot day did not produce absorption spectra of PI fronts.

The positive result, considered the success of this shot day, is that this was the first shot day using this platform and the changes necessary to produce the desired measurements were minimal. In future experiments, a rotation of the target should allow for a standard configuration of the XRS diagnostics, which would remove the concerns about collimation. Holding the capsules at vacuum until minutes before placing them in the chamber should reduce the contamination levels in the capsule spectra. It should also be possible to add measurements, such as x-ray Thomson scattering or x-ray fluorescence, to this platform to allow for more-direct observation of the N. This would allow for redundant measurements that would confirm models for multiple diagnostics. Additionally, with a longer-duration backlighter and a streaked spectrometer, it will be possible to capture the propagation of the PI front with this platform.

This material is based upon work supported by the Department of Energy National Nuclear Security Administration under Award Number DE-NA0003856, the University of Rochester, and the New York State Energy Research and Development Authority.

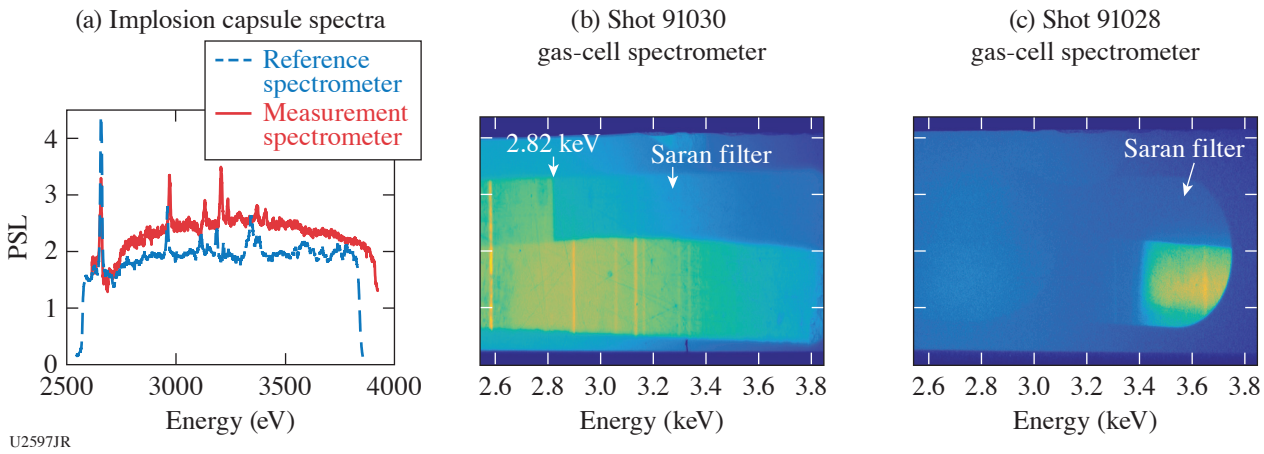

Figure 5
(a) The combined spectral data from both spectrometers on a capsule-only shot. This allows one to compare the emission from the capsule using different lines of sight and shows that it only varies by about 15%. This also shows that the contaminants are not localized to a single location. (b) Raw data from the spectrometer in TIM-3 without a gas cell collimating the capsule emission. It shows a region covered by a Saran filter, which acts as a spectral fiducial from the Cl K edge. (c) The emission seen by the spectrometer in TIM-3 when a gas cell is present demonstrates the collimation of the backlighter and subsequent reduction of the spectral range.

MIT FY19 NLUF Work on High-Energy-Density Physics and Student Training at Omega

Principal Investigator: R. D. Petrasso (MIT)
Co-investigators: C. K. Li, J. A. Frenje, M. Gatu Johnson, F. H. Séguin, and A. Bose (MIT)
Graduate students: P. Adrian, T. Johnson, N. Kabadi, J. Kunimune, B. Lahmann, J. Pearcy, B. Reichelt, R. Simpson, H. Sio, and G. Sutcliffe (MIT)
Undergraduate students: R. Przybocki and H. Propp (MIT)

MIT NLUF work in FY19 included a wide range of experiments applying charged-particle spectrometry, time-history study of inertial confinement fusion (ICF) nuclear and x-ray production, and monoenergetic charged-particle radiography methods developed by MIT and collaborators to the study of ICF plasmas, laboratory astrophysics, and high-energy-density physics (HEDP). Specific major topics where research has produced important results include kinetic and multi-ion-fluid effects on ICF implosion dynamics; ion–electron equilibration in ICF; ion stopping around the Bragg peak in weakly coupled D^3He plasmas; ion stopping in warm dense matter; and nuclear reactions and products relevant to stellar and big-bang nucleosynthesis. Twenty papers about NLUF-related research were published or submitted in FY19,[10,22–40] including seven with MIT first authors.[22,23,32–34,38,40] There were also many invited talks and contributed talks presented at conferences.

Much of the work was done by MIT graduate and undergraduate students in the group; during the last year, the group welcomed two new graduate students (J. Kunimune and B. Reichelt) as part of MIT's long-term program of recruiting and training outstanding Ph.D. students in HEDP and ICF science. Two undergraduates (R. Przybocki of MIT and H. Propp of Cornell) worked with the group and have expressed interest in continuing work in HEDP.

Graduate student H. Sio, after completing his Ph.D. thesis ("Using Time-Resolved Nuclear Diagnostics to Probe Kinetic/Multi-Ion Physics and Shock Dynamics on OMEGA and the NIF"), stayed on as a postdoc to work with student N. Kabadi and LLE collaborators on the development of the particle-x-ray temporal diagnostic (PXTD) that measures the time history of multiple nuclear burn products and multiple energy bands of x-ray emissions in ICF implosions. Dr. Sio has been nominated for the 2020 *Rosenbluth Outstanding Doctoral Thesis Award* for this work. Use of the PXTD has led to the first time-resolved quantita-

tive assessment of the dynamics of fuel-ion species separation in DT^{3}He gas-filled capsule implosions by using simultaneously measured D^{3}He and DT reaction histories.[23,32] These reaction histories captured the relative timing of the nuclear burn histories with unprecedented precision (~10 ps), as seen in Fig. 6(a). Average-ion hydrodynamic simulations, shown in Fig. 6(b), cannot explain the 50±10-ps earlier D^{3}He reaction history relative to DT, even for hydrodynamic-like implosions. The ^{3}He/T fuel ratio in the early phase of the shock burn, inferred from time-resolved D^{3}He/DT yield ratio, is an order of magnitude higher than the initial ^{3}He/T gas-fill ratio and therefore indicates species separation, which obviously cannot be captured by average-ion simulations. As shown in Fig. 6(c), an *LSP* multi-ion simulation captures the timing of these reaction histories. Proposed future efforts will advance these initial studies by exploring the dynamics of kinetic/multi-ion fluid effects and ion-thermal decoupling in D^{3}He and D_2 (with trace T) in shock-driven and ablatively driven implosions.

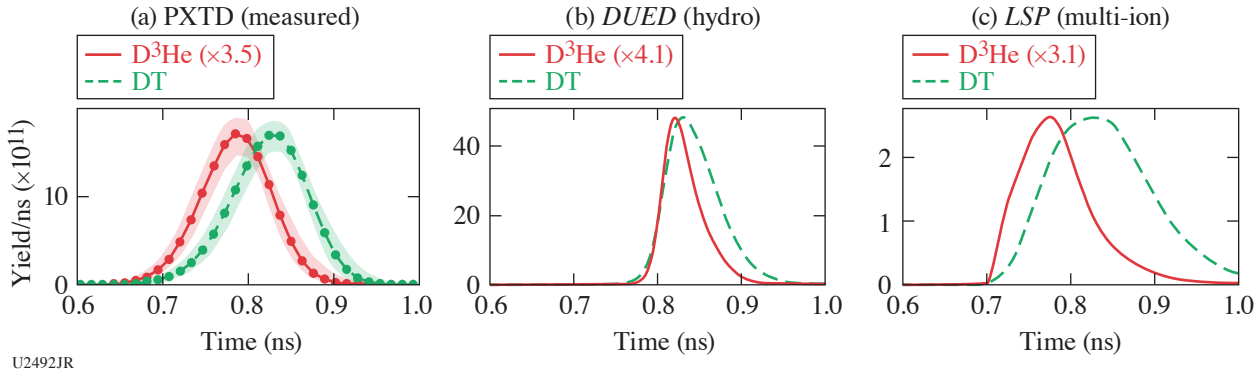

Figure 6
(a) Absolute D^{3}He (red) and DT (green) reaction histories measured with PXTD, (b) simulated by the average-ion hydro-code *DUED*, and (c) *LSP* multi-ion code for OMEGA shot 82615. The D^{3}He reaction histories are amplitude scaled to match the DT histories for clarity. The measured D^{3}He-bang time is 50±10 ps earlier than the DT-bang time. Uncertainties in the PXTD data are indicated by the shaded regions in (a). This work was recently published by former MIT Ph.D. student H. Sio in Physical Review Letters.[32]

Two significant new diagnostic methods that have evolved from students' NLUF science experiments this year will be very important for many future experiments on OMEGA. The first is "cryoPXTD," which is the PXTD modified with improved optics for cryogenic ICF experiments; it will have 10-ps relative timing accuracy of nuclear-burn and x-ray-emission measurements, and it will provide measurements of electron temperature as a function of time. The second method is an extension of the monoenergetic-charged-particle radiography technique for imaging and analyzing plasmas and their self-generated electromagnetic fields, originally developed by MIT scientists C. K. Li, R. D. Petrasso, and F. H. Séguin (who received the 2017 *John Dawson Award for Excellence in Plasma Physics Research* for this NLUF work done on OMEGA). This radiography technique previously utilized a backlighter that supplied 3- and 14.7-MeV protons, but student G. Sutcliffe is developing a new tri-particle backlighter that supplies monoenergetic 9.5-MeV deuterons in addition to the 3- and 14.7-MeV protons. This new backlighter makes it possible to simultaneously record three radiographs (one for each particle type) and thereby provide new options for uniquely identifying the separate effects of self-generated electric and magnetic fields in plasmas imaged with radiography. Student J. Pearcy has already done preliminary work on deducing the spatial distributions of magnetic fields observed indirectly in some of these new radiographs.

Other individuals in the Division have carried out other important new physics studies and received important awards. For example, scientist M. Gatu Johnson (see Fig. 7) was selected as the 2019 recipient of the American Physical Society's prestigious *Katherine E. Weimer Award* for outstanding plasma science research by a woman physicist in the early stages of her career. The citation on her certificate reads, "For significant contributions to Inertial Fusion Sciences and pioneering work in Stellar Nucleosynthesis through nuclear measurements," and much of her work was done on OMEGA through the NLUF program.

Scientist C. K. Li did innovative breakthrough studies on astrophysically relevant, electromagnetic collisionless shocks in the laboratory. These studies led to the definitive demonstration that the structure and dynamics of astrophysical collisionless shocks can be modeled in the laboratory and provided new insight into the role of the Weibel instability in electron heating and shock

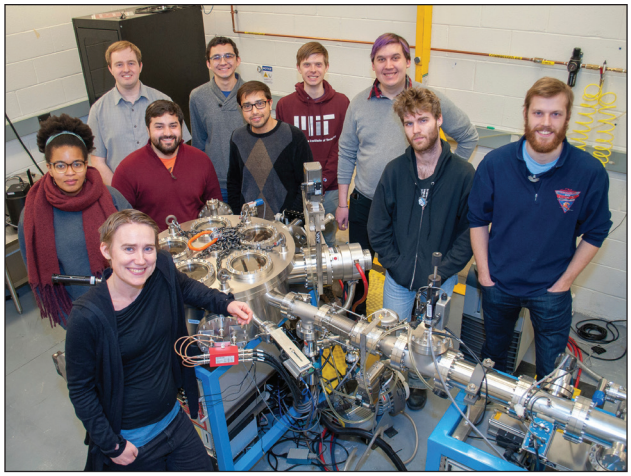

U2494JR

Figure 7
M. Gatu Johnson, 2019 *Weimer Award* recipient, shown with MIT graduate students and MIT's accelerator that is used for ICF diagnostic development.

mediation. Collisionless shocks are ubiquitous in the universe as a consequence of supersonic plasma flows sweeping through interstellar and intergalactic media, and the generation of electromagnetic collisionless shocks in the laboratory has been an important goal during the last several decades for elucidating large-scale astrophysical phenomena (e.g., supernova remnants and protostellar jets), accreting compact objects, and studying a broad range of fundamental physics phenomena. Sponsored by the NLUF program, laboratory experiments led by MIT demonstrated the formation of a quasi-perpendicular, magnetized collisionless shock. The collisionless shock was responsible for electron acceleration to energies exceeding the average energy by two orders of magnitude. These results were recently published by Physical Review Letters.[22]

This material is based upon work supported by the Department of Energy National Nuclear Security Administration under Award Numbers DE-NA0003539 and DE-NA0003539, the University of Rochester, and the New York State Energy Research and Development Authority.

Demonstration of Talbot–Lau X-Ray Deflectometry (TXD) Electron Density Diagnostic in Laser–Target Interactions
Principal Investigators: M. P. Valdivia Leiva (Johns Hopkins University)
Graduate students: M. Trantham and H. Le Fevre (University of Michigan); M. Vescovi (Universidad Catolica de Chile); and V. Bouffetier (University of Bordeaux)

A Talbot–Lau x-ray deflectometer (TXD) electron density diagnostic[41] has been implemented on the OMEGA EP laser. The task was preceded by preparatory experiments on the Multi-Terawatt (MTW) laser. Moiré imaging was demonstrated using a laser-based x-ray backlighter to backlight a static object and a laser-produced plasma object. Measurement of electron density gradient maps of above-quarter-critical density in ablating plasmas (i.e., plasmas actively irradiated by an intense laser) through TXD was pursued.

The OMEGA EP experiment was carried out on 5 December 2018 and tested the TXD technique. The experimental design was carried out in collaboration with Dr. P. Keiter (now at LANL), Dr. P. Drake, and graduate students from the University of Michigan, who also supported the design, preparation, and execution of the OMEGA EP experiment. The irradiated foil experiment was designed along with the diagnostic adaptation for OMEGA EP.

The experiment required design and implementation of a TXD diagnostic platform compatible with the OMEGA EP laser. The project was supported by C. Mileham and C. Stoeckl, among many other science and engineering LLE staff. From the original concept design submitted by Johns Hopkins University and considering TXD diagnostic requirements, LLE's engineering team proposed a rail-like TXD design compatible with a TIM diagnostic setup, which is one of the front ends to the OMEGA EP laser x-ray charge-coupled–device (CCD) imaging camera diagnostic. The final design by J. Zou allows for interferometer alignment using a laboratory x-ray source outside the OMEGA EP chamber. The setup maintains the geometrical conditions once the diagnostic is placed inside the vacuum chamber. The design allows for fine adjustments for potential grating tilting, precise and independent rotation of gratings, as well as small displacement in *xyz*, with a wider range of motion in the *z* direction (see Fig. 8).

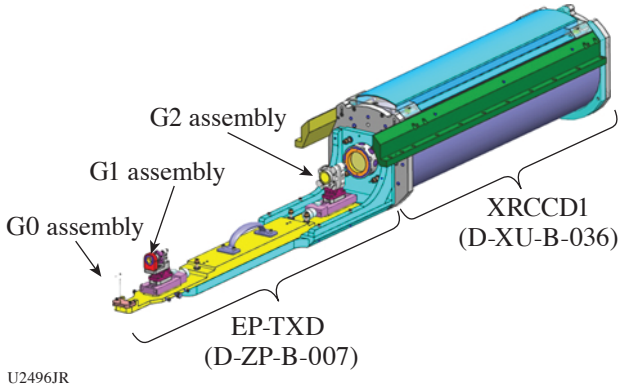

Figure 8
OMEGA EP TXD diagnostic schematic.

Simulations of propagating density profiles from laser–matter interaction of plastic foils were performed [Fig. 9(a)] to better understand thermal electron transport in laser-produced plasmas. Propagation density profiles from laser–matter interaction of plastic (CH) foils were simulated and provided ablation profiles of the laser-irradiated planar foil above critical density. Synthetic Moiré patterns were generated from the simulated electron density profiles and analyzed through the TXD methods. The foil ablation profile expands along the direction shown in Fig. 9(b). TXD imaging will provide an x–y map, and an electron density profile will be detected along the y direction. It should be noted that the Moiré image will also provide vertical electron density information for the radial expansion of the foil along x, albeit with spatial resolution limited by a fringe period. The foil and ablation-front orientation with respect to the grating bars is shown in Fig. 9(c).

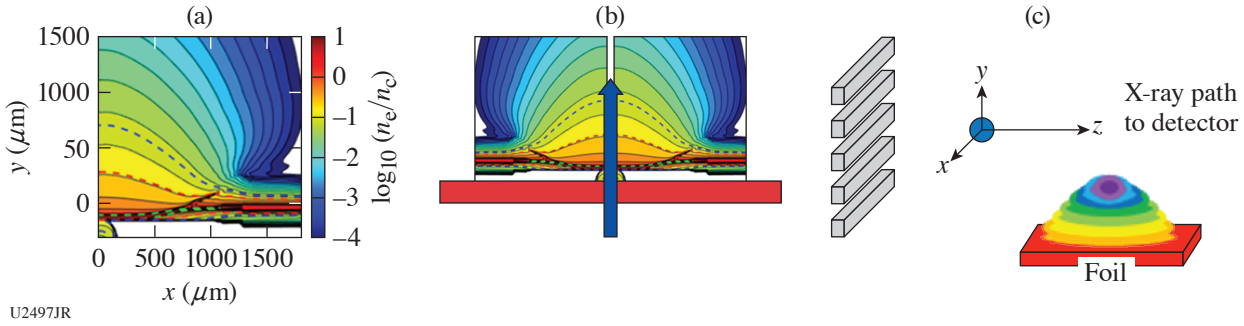

Figure 9
(a) Electron density *CRASH* 2-D simulation; (b) ablation expansion diagram; and (c) measurement schematics for the OMEGA EP experiment showing source grating bars orientation.

The OMEGA EP experiment aimed to demonstrate grating survival for x-ray laser backlighting of <100 J as well as fringe formation. This goal was accomplished, demonstrating laser-based Moiré imaging. A Moiré image was obtained with a 48.7-J, 10-ps, 70-μm-spot-size backlighter beam. A fringe contrast of ~12% to 15% was measured for a backlighter foil to a source grating distance of 2 mm, compared to the 26% to 28% obtained with a Cu x-ray tube. Hard hits reached a level of <21,000 counts, with ~1.8 signal-to-noise ratio. Figure 10 shows a 200-μm × 1.75-mm × 0.5-mm Ta slab. A FWHM of 60.3±2.0 μm was measured by the edge method.

A second goal of the EP-TXD experiment was to obtain electron density profiles from an ablation plasma front. In addition to demonstrating TXD capabilities as an advanced diagnostic for HEDP plasmas, these results were expected to benchmark radiation hydrodynamic codes that fail to predict ablation dynamics in laser-produced plasmas. Following the results shown in Fig. 10, the CH foil was irradiated with three UV beams at maximum energy with a backlighter beam pulse of 48.7 J, 10 ps, and 70-μm spot size. An electromagnetic pulse caused an error in the CCD electronics readout, which rendered the detector unavailable for the remaining laser shots. The x-ray CCD was replaced with image plates; however, since their x-ray energy response is high for higher energies, no discernible fringes were observed, and no Moiré images were recorded from an irradiated foil

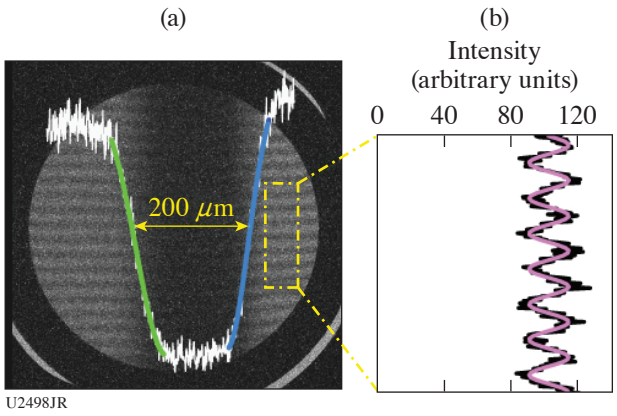

Figure 10
(a) Moiré image of a Ta test object (200 μm × 1.75 mm × 1.5 mm) recorded with the x-ray CCD and (b) the Moiré fringe contrast plot.

ablation front. Therefore, the second goal was not accomplished given that electron density mapping of a plasma object was not achieved. Nevertheless, these results served as a detector capability test for a future EP-TXD diagnostic that will suppress the high-energy component by means of refractive optics. With that goal in mind, a multilayer mirror configuration will be explored in our upcoming NLUF grant.

1. E. N. Parker, *Cosmical Magnetic Fields: Their Origin and Their Activity*, The International Series of Monographs on Physics (Clarendon Press, Oxford, 1979).
2. A. Brandenburg and Å. Nordlund, Rep. Prog. Phys. **74**, 046901 (2011).
3. C. Federrath *et al*., Astrophys. J. **797**, L19 (2014).
4. C. Federrath, J. Plasma Phys. **82**, 535820601 (2016).
5. M. R. Krumholz and C. F. McKee, Astrophys. J. **630**, 250 (2005).
6. C. Federrath and R. S. Klessen, Astrophys. J. **763**, 51 (2013).
7. P. Padoan and A. Nordlund, Astrophys. J. **576**, 870 (2002).
8. P. Tzeferacos *et al*., Phys. Plasmas **24**, 041404 (2017).
9. P. Tzeferacos *et al*., Nat. Commun. **9**, 591 (2018).
10. L. E. Chen *et al*., "Stochastic Transport of High-Energy Particles Through a Turbulent Plasma," submitted to Physical Review Letters.
11. A. F. A. Bott *et al*., to be submitted to Proceedings of the National Academy of Sciences.
12. B. Fryxell *et al*., Astrophys. J. Suppl. Ser. **131**, 273 (2000).
13. A. Dubey *et al*., Parallel Comput. **35**, 512 (2009).
14. P. Tzeferacos *et al*., High Energy Density Phys. **17**, 24 (2015).
15. Flash Center for Computational Science, University of Chicago, Chicago, IL 60637, http://flash.uchicago.edu/site/.
16. C. Graziani *et al*., Rev. Sci. Instrum. **88**, 123507 (2017).
17. A. F. A. Bott *et al*., J. Plasma Phys. **83**, 905830614 (2017).
18. B. Strömgren, Astrophys. J. **89**, 526 (1939).
19. R. P. Drake *et al*., Astrophys. J. **833**, 249 (2016).
20. W. J. Gray et al., Phys. Plasmas **26**, 052901 (2019).

21. J. S. Davis *et al*., Phys. Plasmas **25**, 073304 (2018).
22. C. K. Li *et al*., Phys. Rev. Lett. **123**, 055002 (2019).
23. H. Sio *et al*., Phys. Plasmas **26**, 072703 (2019).
24. D. B. Schaeffer *et al*., Phys. Rev. Lett. **122**, 245001 (2019).
25. T. R. Joshi *et al*., Phys. Plasmas **26**, 062702 (2019).
26. P. Mabey *et al*., Sci. Rep. **9**, 8157 (2019).
27. P.-E. Masson-Laborde *et al*., Phys. Rev. E **99**, 053207 (2019).
28. A. S. Liao *et al*., Phys. Plasmas **26**, 032306 (2019).
29. L. Gao *et al*., Astrophys. J. Lett. **873**, L11 (2019).
30. Y. Lu *et al*., Phys. Plasmas **26**, 022902 (2019).
31. V. Gopalaswamy *et al*., Nature **565**, 581 (2019).
32. H. Sio *et al*., Phys. Rev. Lett. **122**, 035001 (2019).
33. M. Gatu Johnson *et al*., Phys. Plasmas **26**, 012706 (2019).
34. J. A. Frenje *et al*., Phys. Rev. Lett. **122**, 015002 (2019).
35. A. M. Saunders *et al*., Phys. Rev. E **98**, 063206 (2018).
36. G. Kagan *et al*., Contrib. Plasma Phys. **59**, 181 (2019).
37. P. T. Springer *et al*., Nucl. Fusion **59**, 032009 (2019).
38. M. Gatu Johnson *et al*., Phys. Rev. E **98**, 051201(R) (2018).
39. O. M. Mannion *et al*., Rev. Sci. Instrum. **89**, 10I131 (2018).
40. M. Gatu Johnson *et al*., Rev. Sci. Instrum. **89**, 10I129 (2018).
41. M. P. Valdivia *et al*., Rev. Sci. Instrum. **91**, 023511 (2020).